Published in : Semicond. Sci. Technol. **23**, No 12, 125023 (2008) /**DOI** 10.1088/0268-1242/23/12/125023

Coupled Modeling of Current Spreading, Thermal Effects, and Light Extraction in III-Nitride Light-Emitting Diodes

M V Bogdanov[1], K A Bulashevich[1], I Yu Evstratov[1], A I Zhmakin[2] and S Yu Karpov[1]

[1] STR Group – Soft-Impact, Ltd., P.O.Box 83, St.Petersburg, 194156 Russia
[2] Ioffe Physico-Technical Institute, RAS, St.Petersburg, 194021 Russia

E-mail: sergey.karpov@str-soft.com

Abstract. Hybrid approach to modeling of electrical, optical, and thermal processes in state-of-the-art light-emitting diodes (LEDs) is described in detail. The advantages of the approach are demonstrated with reference to an interdigitated multipixel array (IMPA) chip design recently suggested to improve the LED performance at high-current operation. Such an LED, consisting of a hundred single-pixel light sources integrated on a common substrate, has a rather complex multi-scale geometry challenging for a coupled analysis of the device operation. The hybrid approach is found to enable coupled simulation of the current spreading, heat transfer, and light emission in the IMPA LED at a modest demand of computer resources and computing time.

Specific features of the IMPA LED operation are discussed in terms of modeling and compared with those of a conventional square-shaped LED. The impact of current crowding on the uniformity of light emission from the dice of both types is examined. A dramatic difference in the series resistance of the IMPA and square-shaped LEDs is explained on the basis of the current spreading analysis. The active region overheating is found to be a critical factor eventually limiting the output optical power of the square LED. Good agreement between the theoretical predictions and observations is demonstrated, which justifies the use of the hybrid approach.

PACS numbers: 85.60.Jb, 85.60.Bt, 44.90.+, 78.60.Fi, 78.66.Fd

1. Introduction

After the first demonstration of high-brightness blue light-emitting diodes (LEDs) in the early 90s [1, 2], III-nitride semiconductors have soon become the basic materials for visible and ultraviolet optoelectronics. The LED heterostructures are conventionally grown on commercial sapphire or SiC substrates. Cheap sapphire substrates are quite suitable for large-scale production of blue/green LEDs operating at low and intermediate current densities. In turn, rather expensive SiC substrates are employed in the LEDs and laser diodes working at high current densities, where a high thermal conductivity of SiC is crucial for efficient thermal management of the devices [3, 4]. As a compromise between the materials properties and cost, silicon substrates have been recently applied to fabricate visible LEDs [5].

The substrate material largely determines the choice of the LED chip design: planar for sapphire and vertical for SiC. A vertical chip with an n-electrode formed to the back side of the SiC substrate provides a highly uniform current density distribution in the active region. In contrast, a planar LED chip with on-one-side n- and p-electrodes exhibits considerable current crowding near the electrode edges [6, 7, 8, 9, 10] and, as a result, an in-plane non-uniformity of the electroluminescence (EL) intensity. In addition, the non-uniform current spreading in the LED die is predicted to induce a local overheating of the heterostructure, lowering the light emission efficiency and affecting the series resistance of the diode [11]. In turn, the heat generation in an LED depends on the fraction of light absorbed inside the heterostructure. Therefore, adequate modeling of the LED operation generally requires a coupled analysis of the current spreading, heat transfer, light emission in the active region, and its extraction from the die.

Earlier studies of current crowding in LED dice were primarily based on analytical quasi-2D models. They largely focused on the role of the n-contact layer [6] and semitransparent p-electrode [7] in the current spreading over the dice and on searching the electrode configurations that would produce a uniform current density distribution in the active region [8, 9, 10]. Those approaches, however, were capable of providing only qualitative predictions insufficient for device engineering. In addition, details of 3D current density distributions in the LED dice of practical designs still remained obscure because of inherent limitations of the simplified models applied. A much deeper insight into the current-spreading phenomena was provided by first 3D simulations of a 340 nm UV LED with a simple electrode geometry, demonstrating, in particular, a dramatic current localization near the electrode edges and its strong effect on the carrier leakage from the active region [12]. The influence of thermal effects on the 3D current spreading and LED characteristics, like output optical power and series resistance, was recently accounted for in [11] on the basis of the hybrid approach.

State-of-the-art III-nitride LEDs normally utilize chips having essentially three-dimensional geometries and a rather complex electrode configurations. A full model of such devices should consider (i) non-equilibrium carrier injection, their recombination, and light emission in the active region of a multilayer heterostructure, (ii) current

spreading in the LED die, (iii) heat generation inside the die and its transfer to the heat sink, and (iv) emitted light propagation in the die, its absorption in some layers, and extraction from the die, producing a useful optical power. Practically all the above problems are interrelated with each other. In particular, the dopant activation and, hence, the carrier concentration and electrical conductivity of individual layers of the heterostructure are temperature-dependent, as well as the light emission efficiency. This affects the current spreading in the LED die, leading to non-uniform self-heating of the diode. As a result, the light emission from the active region becomes also non-uniform, affecting its extraction from the die, etc. All this generally requires to model the electrical, thermal, and optical processes self-consistently.

A brute-force approach to the solution of a conjugated electro-thermal-optical problem of current spreading, heat transfer, and light emission in the practically used LED dice provided by general-purpose software is frequently inefficient. First, to get a sufficient accuracy, extremely large non-uniform grids are needed (evidently, grid steps for a quantum well (QW) and thick contact layers should differ greatly, as these layers actually have very different dimensions). Second, Cartesian grids could not practically resolve small local geometry features; any refinement of such a grid is extended immediately to the domain boundary, thus increasing considerably the number of the grid cells. A more efficient unstructured grid, being built in a very anisotropic domains (typical aspect ratio of lateral to vertical dimensions is ~100-1000), will contain numerous highly distorted tetrahedra that could result in violation of the discrete maximum principle for elliptic problems, etc.

In order to reduce the computing time, we have recently suggested an approximate hybrid approach [13] that enables full coupled modeling of the LED dice with practically employed designs. This approach is close to that successfully used for analysis of mid-infrared InAs LEDs [14]. Besides, it may be considered as a particular case of a general approach to multi-scale multi-physics problems [15], utilizing a coupled model that consists of a few constituent submodels solved in corresponding subdomains that could overlap. There are two advantages of the hybrid approach: (i) the computational grid may be generated and optimized in each subdomain (and, respectively, for each submodel) independently and (ii) the physical models may be chosen and properly simplified in every subdomain with account of its specific properties or specific properties of the respective submodel. As a result, the conjugated solution of the whole problem would require much less computer resources and much shorter computing time, making feasible coupled analysis of electrical, thermal, and optical processes underlying the operation of III-nitride LEDs.

In this paper, we report on application of the hybrid approach to modeling of a multi-pixel violet LED recently suggested to improve the device performance at high-current operation conditions [16]. Such a complex LED design is intentionally chosen in order to demonstrate the capabilities of the hybrid approach in modeling of advanced optoelectronic devices. The simulations provide a better understanding of the processes occurring in such and conventional square-shaped LED considered as a reference case.

The theoretical results are compared with the data reported in [16], providing a detailed validation of the hybrid approach.

The paper is organized as follows. Sec.2 contains a detailed description of the hybrid approach used in this study. The simulation results are discussed in Sec.3. The summary of the study and main conclusions are given in Sec.4.

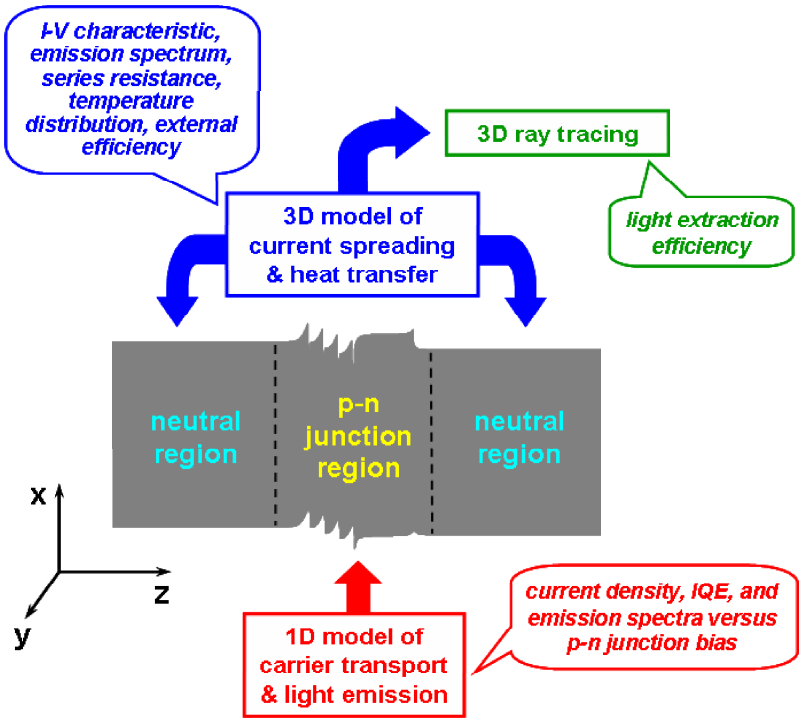

Figure 1. Schematic of hybrid approach to LED modeling. The bandgap profile in a multiple-quantum-well LED structure is shown by gray shadow where electrically neutral n- and p-contact regions with the flat conduction and valence bands and a *p*-*n* junction region (zone) are selected.

2. Model

2.1. Modeling approach

To simulate the current spreading in an LED die, we identify first in the whole LED heterostructure electrically neutral *n*- and *p*-regions (see Fig.1) where the carrier drift dominates over diffusion and the carrier recombination does no longer affect the transport of the majority carriers. The electron current density $\mathbf{j}_n$ obeys in the *n*-region the continuity equation

$$\nabla \cdot \mathbf{j}_n = 0 \quad , \quad \mathbf{j}_n = \mu_n n \nabla F_n \quad , \tag{1}$$

while a similar equation is valid for the hole current density $\mathbf{j}_p$ in the *p*-region

$$\nabla \cdot \mathbf{j}_p = 0 \quad , \quad \mathbf{j}_p = \mu_p p \nabla F_p \quad . \tag{2}$$

Here, n and p are the concentrations of electrons and holes in the neutral n- and p-region, respectively, μ_n and μ_p are the mobilities of the carries, and F_n and F_p are the electron and hole quasi-Fermi levels. The expressions for $\mathbf{j}_n$ and $\mathbf{j}_p$ in Eqs.(1) and (2) actually represent the Ohm law extended to the case of isotype n-n^+ or p-p^+ junctions with negligible non-linearity in their current-voltage characteristics. In a uniform neutral region with flat bands, the gradient of a quasi-Fermi level becomes equal to the gradient of electric potential that governs the majority carrier transport. Being linear, Eqs.(1) and (2) can be easily solved on a 3D-grid, using advanced numerical algorithms.

The neutral n- and p-regions are separated from each other by a thin p-n junction region (or zone) that contains a single-quantum-well (SQW) or a multiple-quantum-well (MQW) active layer with adjacent space-charge regions. The processes in the p-n junction zone are considered within a 1D drift-diffusion approach, accounting for the non-equilibrium carrier injection, their non-radiative and radiative recombination, and light emission. Both spontaneous and piezo-polarization inherent in wurtzite semiconductors are taken into account in the Poisson equation for electric potential. A comprehensive discussion of the model used for the 1D simulations is given in [17]. This paper contains also a list of materials parameters used in our simulations.

Only a small amount of information coming from the 1D modeling is required to simulate the current spreading in the LED die. First, that is the dependence of the vertical current density j_z on the p-n junction bias $U_{p-n} = (F_n^0 - F_p^0)/q$ and temperature T , where q is the electron charge, and F_n^0 and F_p^0 are the values of the electron and hole quasi-Fermi levels at the n- and p-sides of the p-n junction zone, respectively, obtained from the 1D modeling. Another important characteristic is the dependence of the internal quantum efficiency (IQE) $\eta_{\rm int}$ of the LED heterostructure on j_z and T . The IQE is defined as

$$\eta_{\rm int} = \frac{q}{j_z} \int_{p-n \text{ zone}} dz \cdot R_{\rm rad}(z) \quad , \tag{3}$$

where $R_{\rm rad}$ is the radiative recombination rate integrated in (3) over the p-n junction zone. Such a definition accounts for not only the competition between the radiative and non-radiative recombination channels but also possible carrier leakage from the p-n junction zone.

Neglecting the in-plane carrier transport in the thin p-n junction zone, one can parameterize results of the 1D modeling and replace this subdomain by an effective interface that couples n- and p- neutral-region domains via the following boundary conditions

$$\mathbf{n} \cdot \mathbf{j}(\pm 0) = j_z(T, U_{p-n}) \quad , \quad qU_{p-n} = F_n - F_p \tag{4}$$

Here, $\mathbf{n}$ is the normal vector to the interface plane directed from the p- to n-neutral region, and the notations '-0' and '$+0$' correspond to the values of variables at the interface in the n- and p-neutral region, respectively. At free semiconductor surfaces,

the electron and hole current densities are required to equal zero, i. e. the surface recombination is neglected.

Thin metallic electrodes semitransparent for emitted light are frequently deposited on the top of the p-contact layer, if the light is extracted through the top surface of the LED die. To predict correctly the LED series resistance in this case, it is important to account for the current spreading in the metallic electrode along with the current spreading in the die. This is made by solving the 2D equation with respect to the electron Fermi level F_m in the metal:

$$\nabla(\sigma_m \nabla F_m) = -q j_{\rm ex}/h \quad , \quad j_{\rm ex} = (F_m - F_p)/q\rho_p \quad . \tag{5}$$

Here $j_{\rm ex}$ is the density of exchange current outgoing from the metallic electrode to the semiconductor contact layer, h is the electrode thickness, and σ_m is the electric conductivity of the electrode metal. The exchange current density is determined in Eq.5 in accordance with the model of Ohmic contact having the specific resistance ρ_p . In this case, the boundary condition for Eq.(2) set at the interface between the p-contact layer and p-electrode reads

$$\mathbf{n} \cdot \mathbf{j_p} = j_{\rm ex} \quad , \tag{6}$$

where the normal vector $\mathbf{n}$ is directed from the metal to p-semiconductor. A similar boundary condition is also set at the interface between the n-contact layer and n-electrode.

The n- and p-electrode pads are considered as equipotential areas inside the n- and p-electrode domains where $F_m = 0$ and $F_m = qU_f$, respectively; U_f is the forward voltage (bias) applied to the LED.

Thus, the current spreading problems is reduced to self-consistent solution of Eqs.(1), (2), and (5) with the boundary conditions (4) and (6) accounting for the current exchange between the n- and p-neutral regions and n- and p-metallic electrodes. The exchange currents j_z and $j_{\rm ex}$ connect the current densities in the neutral n- and p-regions with the differences of the Fermi levels on the both sides of the respective interface.

The heat transfer is simulated within a conventional 3D approach, considering the non-uniform current density distribution in the LED die. For this purpose the equation

$$\nabla(\kappa \nabla T) = Q \tag{7}$$

is solved to find the distribution of temperature, T , in the LED die. Here κ is the materials thermal conductivity and Q is the heat source density. Both Ohmic heating of the materials bulk, the heating caused by the non-equilibrium carrier thermalization in the p-n junction region, and that related to the emitted light absorption in the LED structure are included in the model as the principal heat sources. The constant thermal conductivity of GaN, $\kappa = 120$ W/K·m [18], is used for modeling the heat transfer in the LED dice.

At the external chip surfaces, either temperature or a heat transfer coefficient and an ambient temperature are prescribed. The thermal analysis is coupled with the current-spreading simulation via the temperature-dependent electrical conductivity of the neutral regions and the dependence $j_z(T, U_{p-n})$. In turn, the temperature dependence of the electric conductivity accounts for both the thermal activation of donors and acceptors and the temperature dependence of the carrier mobilities. The latter have been obtained by approximating the experimental data on electron and hole mobilities in GaN reported in [18]. As soon as the coupled current-spreading and heat-transfer problems are solved, the local power density P_{rad} of light emitted in the *p-n* junction region can be determined as

$$P_{\text{rad}} = (\hbar\omega/q)\eta_{\text{int}} j_z \quad , \tag{8}$$

where $\hbar\omega$ is the energy of emitted photons.

Three-dimensional ray tracing accounting for the non-uniform emission intensity distribution in the active region is then applied to estimate the light extraction efficiency from the LED die and the radiation pattern. The ray tracing is performed in the whole die, including both the heterostructure and substrate. The number of rays emitted from an elementary area of the active layer is chosen to be proportional to the emission intensity. Ray propagation through the chip is monitored until the ray leaves the computational domain or decays considerably because of the light absorption inside the die.

Generally, there are two alternative approaches to treat the ray reflection and refraction at an interface separating the media with different refraction indexes. It is possible either to trace both reflected and refracted rays outgoing from every interface or to incorporate a special random process into the procedure to decide which of these two rays should be further traced in accordance with the value of the transmission and reflection coefficients. The former approach requires allocation of a considerable amount of operative memory to carry out the ray tracing. The latter one needs a larger number of trials to provide a proper statistical averaging. We have chosen the latter approach in the present work, as it turned out to be more efficient. Specular ray reflection at every interface and the absence of diffused scattering was assumed in this study. The value of the GaN refractive index necessary for the ray-tracing analysis is determined from the approximation of its spectral dependence derived in [19].

The above hybrid approach has been implemented in the commercial package SimuLED [20] consisting of three modules. One of the modules, SiLENSe, enables 1D analysis of the LED heterostructure operation, providing the input information for the SpeCLED module and additional results useful for assessment of the heterostructure design. The SpeCLED module solves the coupled current-spreading and thermal problems. The latter results are used, in turn, in the 3D ray-tracing analyzer, RATRO, that predicts the radiation pattern of an LED die and the light extraction efficiency.

2.2. Applicability of hybrid approach

Consider main assumptions and simplifications underlying the hybrid approach and their applicability to III-nitride LEDs. The principal simplification is that the carrier transport and recombination in the core of the LED structure (p-n junction region) is considered withing a 1D approach. Actually, this means that we neglect the lateral electron and hole transport in the active and surrounding layers. The lateral transport is driven by the lateral gradients of the electric potential and carrier concentrations that vary remarkably on the the so called current-spreading length L, being of ∼50-100 μm, as shown below in Sec.3.2. In contrast, the variation of the electric potential and carrier concentrations in the vertical direction occurs on the length less than the total thickness of the heterostructure core D, which does not normally exceed ∼100-200 nm. Since $D << L$, the vertical gradients are much greater than the lateral ones. This justifies the use of 1D approximation for the carrier transport in the core of LED structure.

Another assumption is substitution of the bipolar conductivity in the n- and p-contact layers by the unipolar one, which enables to use the Ohm law, i. e. Eqs.(1)-(2), for computation of the electron and hole current densities. The bipolar conductivity becomes important at high current densities, where the carrier leakage from the heterostructure core is strong enough (see discussion in Sec.3.1). In the case of extremely strong leakage, the actual conductivity of a contact layer may differ from that assumed in simulation by the factor of two. From the practical point of view, however, the carrier leakage is undesirable effect which should be avoided by device engineering rather than simulated accurately. Therefore, the current spreading model, using unipolar conductivity instead of the bipolar one, provides quantitatively accurate results for the low-leakage conditions and describes qualitatively well the device operation at high leakage. In principle, the model predictability may be additionally improved by extending the p-n junction (core) region in such a way, as to include the contact layer where the carriers leak to. In this case, the bipolar conductivity in the contact layer can be accounted for within the 1D approach.

Among other shortcomings of the hybrid approach are those typical for drift-diffusion model of the electron and hole transport in device heterostructures. Namely, they are ignoring of ballistic transport in very thin semiconductor layers and hot-carrier effects, neglecting the quantum-confinement effects while computing the band diagram and carrier recombination rates, etc. These drawbacks of drift-diffusion approach are well known and repeatedly discussed in literature. Unfortunately, up to now there are no good alternatives that would be capable of robust and effective working in the case of state-of-the-art devices, normally having a complex multi-scale 3D geometry. In our simulations we also neglect the possible avalanche carrier multiplication in the p-n junction region despite the extremely high electric field induced by the polarization charges at the heterostructure interfaces. This can be done, since the layers in the core of the LED structures are sufficiently thin.

Finally, the ray-tracing used for prediction of the light extraction efficiency from

LED dice and radiation patterns neglects the light interference in the heterostructure, though it can be important in some cases [21]. Accounting for the wave nature of light in the ray-tracing procedure is a rather challenging task that requires further developments.

3. Results

Following [16], we compare LEDs with IMPA and conventional square chip designs. Both LEDs utilized the same heterostructure grown on a basal-plane sapphire substrate. The structure contained a 2 μm Si-doped n-GaN contact layer followed by the active region, which consisted of a five 5 nm $In_{0.08}Ga_{0.92}N$ quantum wells separated by 32 nm Si-doped GaN barriers. A 15 nm Mg-doped $Al_{0.2}Ga_{0.8}N$ layer placed between the active region and p-GaN contact layer was used as a blocker of electron leakage. The structure was capped with a 200 nm Mg-doped p-GaN contact layer. The donor concentration in the n-GaN contact layer ([Si] = 3×10^{19} cm^{-3}) was estimated from the sheet resistance reported in [16]. We also assume the donor concentration in the barriers to be of 5×10^{18} cm^{-3} and the acceptor concentration in the p-AlGaN and p-GaN layers to be of 1.5×10^{19} cm^{-3} and 2×10^{19} cm^{-3}, respectively. These values are typical for LED heterostructures used in practice. The LED heterostructure provided the emission spectrum peaked at 400 nm.

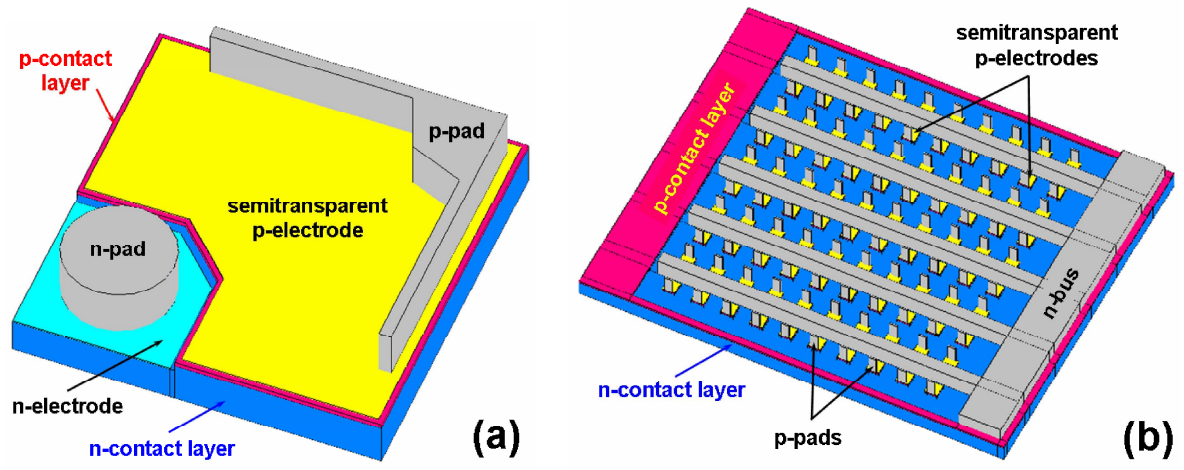

Figure 2. Three-dimensional geometries of square-shaped (a) and IMPA (b) LED dice used in simulation.

The IMPA die consisted of a hundred of 30×30 μm^2 pixel-LEDs integrated on a common sapphire substrate. The detailed description of the IMPA design and its fabrication procedure was discussed in [16]. The IMPA chip utilized a common p-bus deposited on a dielectric film serving for insulation. As such 3D overlapping configurations are not allowed in the SimuLED package, we substitute the p-bus by micro p-pads formed to the p-electrodes on the top of every pixel LED (see Fig.2b). The square die was not specified in [16] with sufficient detail. Therefore, we have chosen

a rather typical electrode configuration shown in Fig.2a. Both dice had equal light emitting areas but the total IMPA die area was approximately ten times larger than that of the square die. The n- and p-contact resistances were $5 \times 10^{-5}\ \Omega \cdot \mathrm{cm}^2$ and $1 \times 10^{-3}\ \Omega \cdot \mathrm{cm}^2$, respectively, as reported in [16].

3.1. Operation of LED heterostructure

Modeling of electron and hole injection and light emission in the LED heterostructure has been performed with the SiLENSe 3.0 package [20]. The model accounts for the carrier transport in the heterostructure within a drift-diffusion approach and considers the non-radiative carrier recombination at point defects with the electron and hole life times of 50 ns, the bimolecular radiative recombination with the recombination constant $B = 2.26 \times 10^{-11}\ \mathrm{cm}^3/\mathrm{s}$, and the Auger recombination in InGaN QWs with the Auger coefficients $C_p = C_n = 2.4 \times 10^{-31}\ \mathrm{cm}^6/\mathrm{s}$. The non-radiative carrier recombination at threading dislocations is also accounted for in the model with the electron and hole life times depending on the dislocation density, in accordance with [22]. The dislocation density was assumed to be of $10^9\ \mathrm{cm}^{-2}$ in all the layers except for the InGaN quantum wells where it was set an order of magnitude lower, which roughly accounts for the effect of composition fluctuations on the InGaN alloys (see [17] for details).

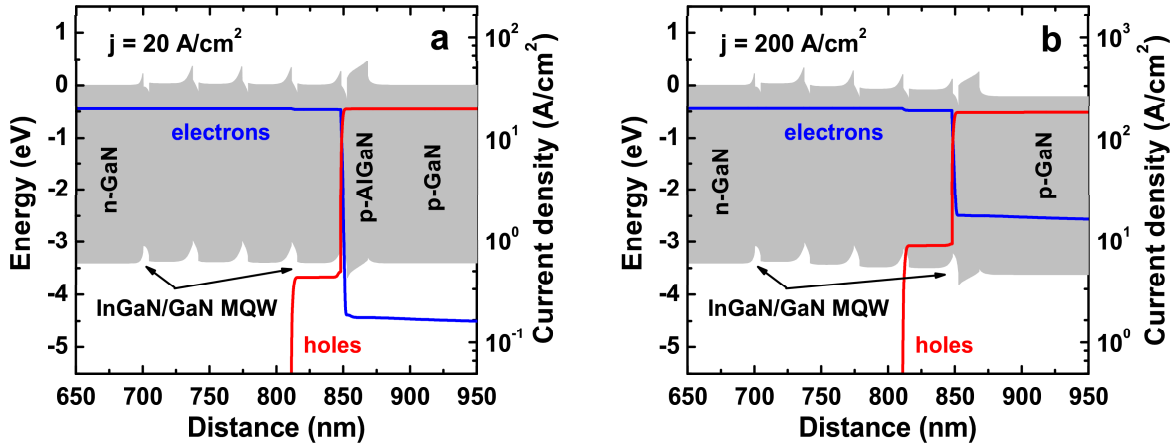

Figure 3. Room-temperature band diagrams and partial electron and hole current densities in the LED heterostructure operating at the current density of 20 $\mathrm{A/cm}^2$ (a) and 200 $\mathrm{A/cm}^2$ (b).

The computed band diagram of the LED heterostructure and the partial electron and hole current densities corresponding to the total current density j_z of 20 and 200 $\mathrm{A/cm}^2$ are shown in Fig.3 One can see that the conduction and valence bands in the p- and n-GaN contact layers, as well as in the n-GaN barriers separating the InGaN quantum wells, are nearly flat at such current densities. This means the electric field to remain unscreened only in the p-AlGaN blocking layer, quantum wells, and narrow space-charge regions adjacent to the wells.

One can realize from the partial current density distributions in Fig.3 that electrons can easily penetrate through the multiple-quantum-well active region at high current densities, partly leaking into the p-GaN contact layer. The reason for the leakage is the lowering of the potential barrier formed in the AlGaN blocking layer with the current density. For $j_z = 20$ A/cm^2 , the simulation predicts the electron leakage current to be less than 1% of the total current through the diode. In contrast, for $j_z = 200$ A/cm^2, about 9% of electrons are lost at the p-electrode because of the leakage. At higher current densities and higher temperature, the electron leakage becomes even more pronounced, considerably reducing the internal quantum efficiency of the LED structure.

The hole current density becomes negligibly small when holes pass through the quantum well adjacent to the AlGaN blocking layer. As a result, only this well is filled sufficiently with holes, giving the major rise to the radiative carrier recombination. Actually, more than 95% of all photons are emitted from the well, while other QWs are inefficient for light emission.

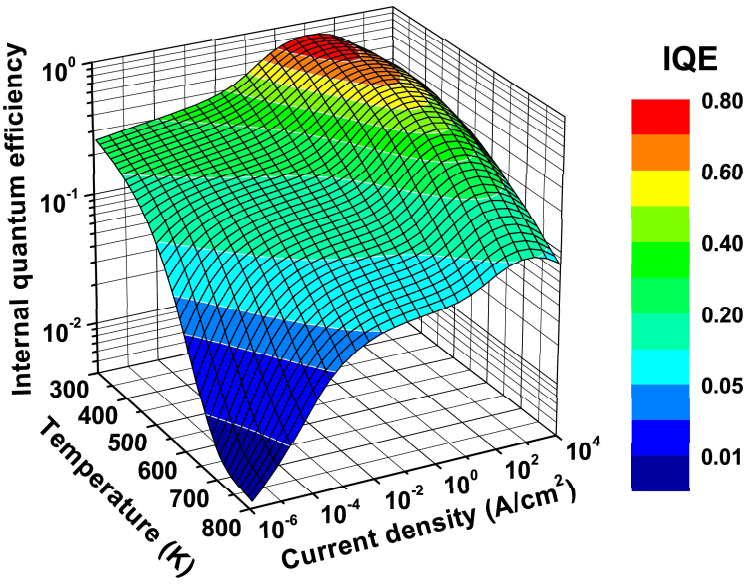

Figure 4. IQE of the LED heterostructure as a function of current density and temperature.

IQE of the LED structure is found to depend non-monotonically on the current density and to decrease gradually with temperature (Fig.4). The IQE reduction at high current densities is caused by contribution of both the electron leakage from the active region and Auger recombination to the carrier losses. The IQE variation with temperature is related to the specific temperature dependences of both radiative and non-radiative recombination rates.

3.2. Characteristics of LED dice

Simulation of the current spreading and heat transfer in the square LED die has been performed with the SpeCLED 2.0 package on a 3D in-plane unstructured grid consisting of 85 000 cells. A hybrid 3D structured/unstructured grid with 535 000 cells has been used for the IMPA LED modeling. The temperature dependence of the carrier mobilities and activation degrees of donors and acceptors in the n- and p-contact layers was accounted for in the simulations. The heat transfer coefficient of 30 W/cm^2·K was set at the back side of the LED structure, which corresponds to the thermal resistance of the 150 μm sapphire substrate.

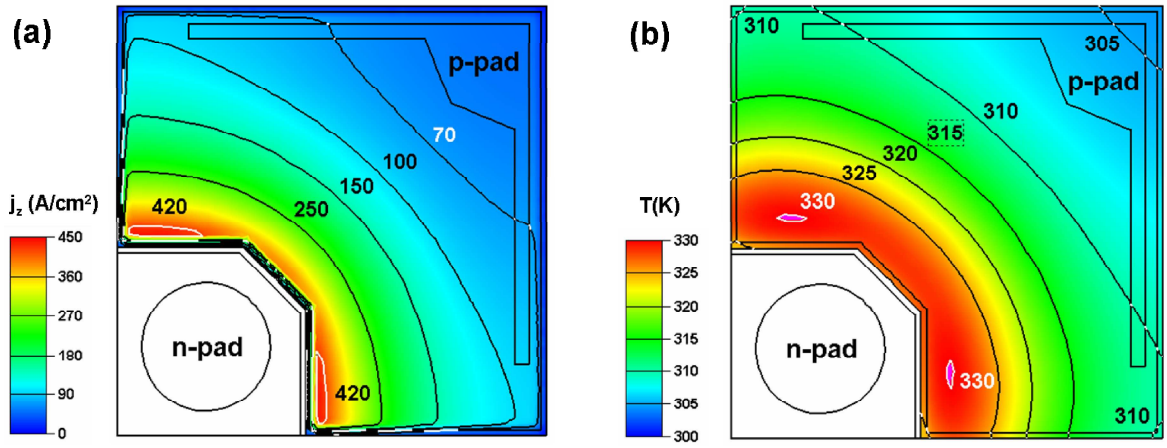

Figure 5. Current density (a) and temperature (b) distributions in the active region of the square LED. The digits marking isolines correspond to the current density and temperature measured in A/cm^2 and K, respectively.

Figure 5 displays the computed distributions of the current density and temperature over the active region of square LED at the forward current of 100 mA. One can see that the current crowding occurs near the gap between the n- and p-electrodes. The current density decays nearly exponentially with the distance measured from the p-electrode edge. The specific decay (or current-spreading) length L is found to weakly depend on the current flowing through the diode. It is of ~80 μm at 50 mA and ~70 μm at 500 mA. The current-spreading length determined in this study is about 3 times smaller than that derived in [16] on the basis of analytical estimates. Such a big discrepancy between the values of the current-spreading length shows that the analytical estimates may be inadequate because of ignoring the non-linear character of the current crowding caused by interrelation of the electrical and thermal processes.

The local overheating of the active region originates from the current crowding near the inter-electrode gap. The maximum temperature approaches here ~450 K at 300 mA and ~650 K at 500 mA. The active region overheating results in a reduced IQE of the LED structure and, eventually, in the optical power rollover, as discussed below.

Comparison of simulated and experimental current-voltage characteristics of the

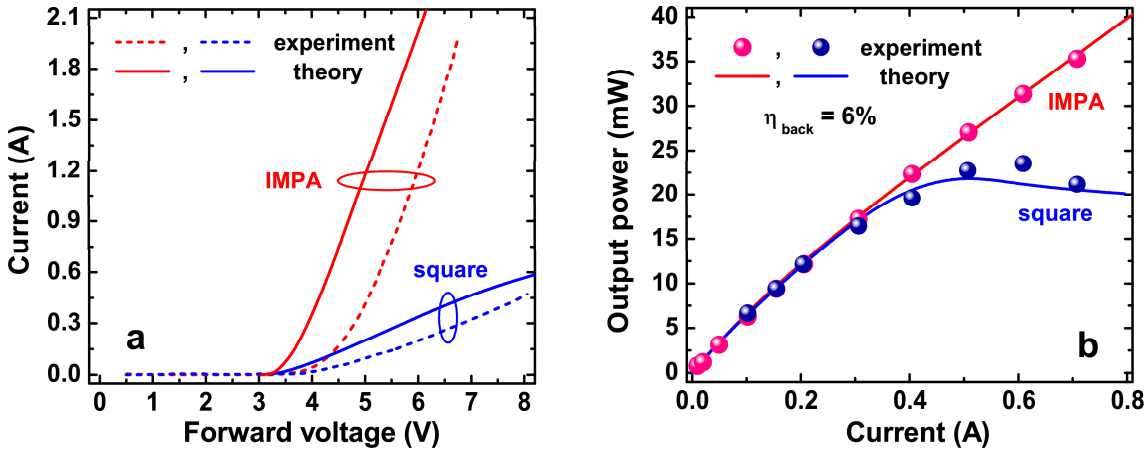

Figure 6. Experimental and theoretical current-voltage characteristics (a) and output optical power as a function of current (b) for square and IMPA LEDs.

square and IMPA LEDs is given in Fig.6a. The simulations reproduce quantitatively well the observed reduction of the LED series resistance (from ∼7-9 Ω to 1.2 Ω) due to the use of the IMPA chip design. The theoretical values of the series resistance agree well with those of 8 Ω and 1 Ω reported in [16] for the square and IMPA LEDs, respectively. However, the turn-on voltage, 3.2 V, obtained by modeling is lower than the experimental one, ∼3.9 V. Since the former value corresponds well to various literature data on InGaN LEDs, we attribute this discrepancy to additional barriers formed in the LED in course of its fabrication. For instance, is may be a barrier related to the non-ohmic behavior of the p-contact.

In order to understand the large difference between the series resistances of the square and IMPA LEDs, we assume that it is primarily determined by the the current spreading in the n-contact layer. Then the series resistance can be roughly estimated as $R_s \approx L/\sigma P d$, where σ is the electric conductivity of the n-contact layer, d is the n-contact layer thickness under the n-electrode, and P is the electrode perimeter, through which the current effectively flows in the lateral direction. At $d = 1.7$ μm and $p = 240$ μm (which was obtained from the electrode geometry), the estimation provides the series resistance of ∼7 Ω for the square LED, in good agreement with numerical modeling and experiment. In the case of the IMPA LED, the current spreading length should be taken equal to the side length of an individual pixel, i.e. to 30 μm. Then at $p = 1800$ μm (the length of a p-pad multiplied by the number of pixels), the estimated series resistance is about 0.4 Ω, which is three times lower than the value obtained by simulation. This discrepancy may be addressed to the contribution of the p-contact layer resistance that was neglected in the above rough estimate. Nevertheless, the estimate clearly shows that the series resistance is primarily controlled by the electrode perimeter which is much larger for the IMPA LED.

The output power of light emitted from back side of the sapphire substrate

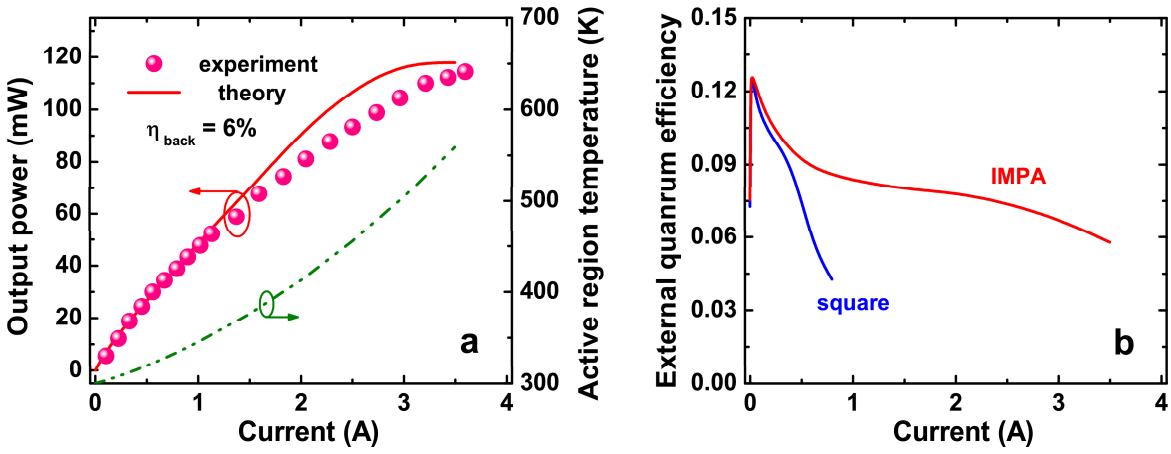

Figure 7. Output optical power and active layer temperature in the IMPA LED (a). Comparison of the external quantum efficiencies of square and IMPA LEDs (b).

computed for the square LED operated at different currents reproduces well the rollover observed in [16] at the currents greater than 0.6 A (Fig.6b). This effect is primary related to the device self-heating (the average active layer temperature is predicted to reach ∼450 K, while the maximum temperature approaches ∼800 K at this current). The IMPA LED has a much better heat sink, primarily due to a larger die area. As a result, no rollover of the emission power is predicted for the IMPA LED even at the current as high as 3.5 A (see Fig.7a), in line with the data of [16]. The active layer temperature in the IMPA LED approaches ∼580 K at 3.5 A with a 5% difference between the pixels in the centre and on the periphery. The current density is as high as 3.9 kA/cm^2 at this current and is very uniformly (within ∼1%) distributed among the individual pixels. In turn, this provides a very small scatter of the emission wavelength and electroluminescence intensity between different pixels, which agrees well with the observations made in [16].

Figure 7a compares the computed and measured output optical power of the IMPA LED in a wide range of the forward current variation. One can see that the theoretical curve lies above the experimental points at the current higher than 1.5 A . As the disagreement becomes noticeable at the conditions where the active region is remarkably overheated, we attribute it to insufficiently accurate approximation of temperature dependence of materials properties, like the carrier mobilities and Auger recombination coefficients.

Figure 7b shows the simulated external quantum efficiencies of both square and IMPA LEDs as a function of the forward current. This plot clearly demonstrates the advantages of the IMPA chip design over the square one. Due to suppressed current crowding and reduced overheating, the IMPA LED is capable of high-current operation without considerable droop of the external efficiency at the currents from 1 to 3 A.

3.3. Light extraction from LED dice

To compute the light extraction efficiency and radiations pattern of the LEDs, the 3D ray-tracing has been performed, using 20 million probe rays and accounting for the non-uniform emission intensity distribution in the LED active regions. A 150 μm sapphire substrate was allowed for in the simulations. No diffuse component of light reflection from all the available surfaces was considered in this study, i. e. all the surfaces were regarded as specular reflecting. We also assumed that the emitted light was strongly absorbed in the p-GaN contact layer (with the absorption coefficient of $\sim 5\times10^3$ cm^{-1}). According to the experimental setup used in [16], we considered air to be the ambient medium surrounding the LED dice.

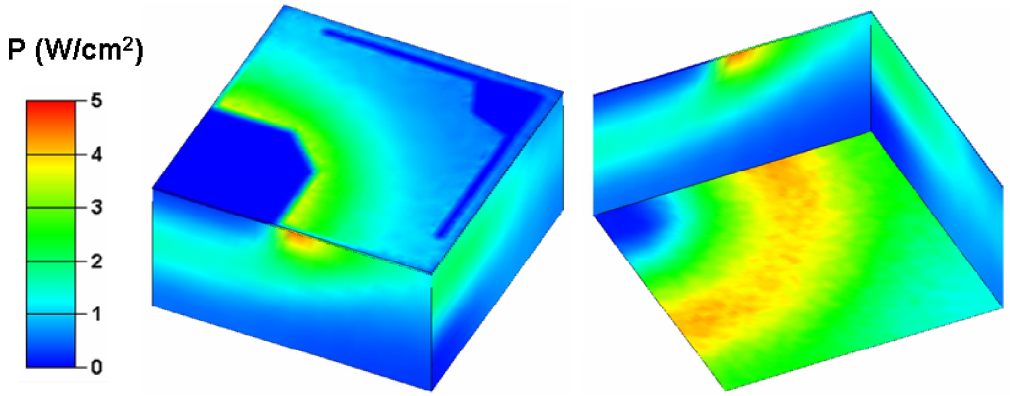

Figure 8. Distributions of the emission power density over the square die surfaces at the forward current of 100 mA: view from the top (a) and view from the bottom (b).

Figure 8 shows the near-field distribution of the emitted optical power over the surfaces of the square LED die. One can see that the light emission from the top die surface (through the semitransparent p-electrode) is quite non-uniform: the light goes out primarily from the region adjacent to the inter-electrode gap, in accordance with the current density distribution shown in Fig.5b. The light extracted from the back sapphire surface is more uniform, though some footprint of the current crowding near the electrode edge is still noticeable. There is also strong light extraction through the side walls of the sapphire substrate, resulting in the far-field radiation pattern different from the Lambertian one [23]. In addition to the strong emission in the region near the electrode edge, one can also see in Fig.8 the light outgoing from the remote side wall of the substrate. This is caused by the waveguiding effect enhancing the propagation of the emitted light along the heterostructure layers, which is related to the large difference between the refractive indexes of n-GaN contact layer (2.58) and sapphire (1.78).

The predicted total light extraction efficiency from the square LED is about 15%. Approximately 3% and 6% of all photons are emitted though the top and back surfaces of the die, while the rest 6% of photons goes out through the side walls of the sapphire substrate. We should note that the predicted output power of the square LED shown

in Fig.6b is obtained just with the account of the light extraction efficiency through the back sapphire surface $\eta_{\text{back}} = 6\%$. This corresponds to the experimental setup in [16] where the only optical powe of light outgoing through the substrate back side was registered.

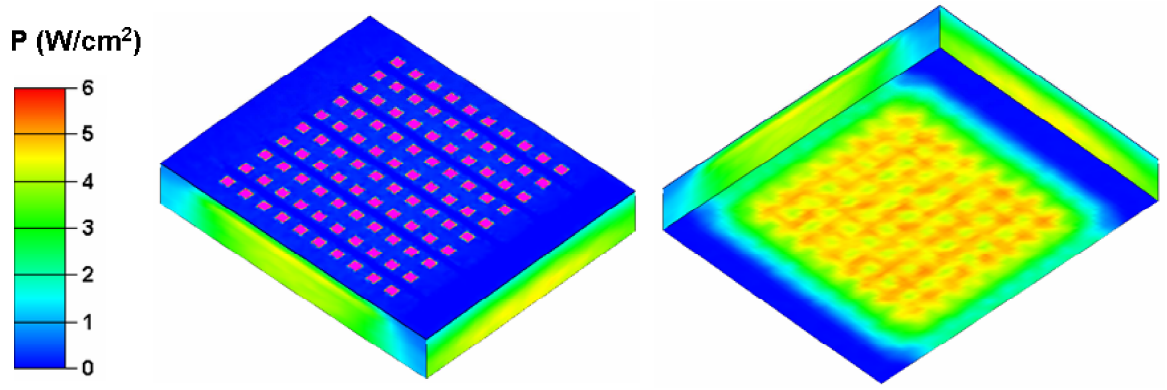

Figure 9. Distributions of the emission power density over the IMPA die surfaces at the forward current of 1 A: view from the top (a) and view from the bottom (b).

The near-field distribution of the emitted optical power over the surfaces of the IMPA LED die is displayed in Fig.9. The top light emission is very uniformly distributed among the individual pixels, which correlates well with observations made in [16]. The ∼15-20% non-uniformity of the back-side emission still manifests specific features of the die design, though it is much more uniform than in the case of the square LED. As previously, there is strong light extraction through the substrate side walls, largely controlled by the waveguiding effect.

From the ray-tracing analysis, we obtain for the IMPA LED nearly the same total light extraction efficiency, as well as the percentage of light extraction through the top and back surfaces and side walls of the sapphire substrate. This conclusion correlates with the data on the output optical power reported in [16].

4. Conclusion

We have applied the hybrid approach to analyze operation of an LED with a novel interdigitated multipixel array (IMPA) die design recently suggested in [16]. The approach involves coupled solution of problems with different dimesionalities, from 1D to 3D, which allows considerable reduction of the computing time. The results obtained by using the hybrid approach agree well with available data.

The LED heterostructure used for the IMPA LED fabrication is found to provide inefficient suppression of the electron leakage at high current densities that lowers the IQE of light emission. Additional IQE reduction under high-current operation conditions is caused by the Auger recombination of non-equilibrium carriers. Only one of five

quantum wells, which is adjacent to the p-AlGaN blocking layer, gives the major rise to the light emission, while other wells are largely depleted with holes.

The current spreading and heat transfer simulation show that the IMPA LED avoids the current crowding in the die and provides a much lower overheating of the active region. The former is due to the chosen dimensions of the p-electrode pixels, which are much smaller than the typical current spreading length in such LEDs. The latter is largely related to a larger total area of the IMPA chip, providing much better heat sink for the diode. Both factor are extremely important for high-current operation of the IMPA LED, resulting in a comparably low droop of the external quantum efficiency with current.

The square and IMPA LEDs considered here have the light extraction efficiency more or less typical of III-nitride LEDs with flat heterostructure/substrate interfaces and outward surfaces. The use of conventional approaches, like profiling of the sapphire substrate before growth of the LED structure, texturing of the emitting surfaces, etc. would allow further increase of the external efficiency.

Our simulations predict the temperature distribution in the LED dice to be quite non-uniform because of the current crowding. This non-uniformity may produce a strong thermo-elastic strain in the LED structure, eventually resulting in additional built-in piezo-polarization field. To what extent this additional electric field may interfere the carrier transport in the contact layers of LED dice, is still an open question. We think, it should be addressed by further studies. However, this may require to employ an extended statement of the whole problem accounting not only the temperature non-uniformity by itself but also the wafer bending occurring during the heterostructure growth and the manner of the die mounting on the heat sink, both affecting the induced strain.

References

[1] Nakamura S 1994 Zn-doped InGaN growth and InGaN/AlGaN double-heterostructure blue-light-emitting diodes *J. Cryst. Growth* **145** 911-7

[2] Nakamura S, Mukai T, and Senoh M 1994 Candela-class high-brightness InGaN/AlGaN double-heterostructure blue-light-emitting diodes *Appl. Phys. Lett.* **64** 1687-9

[3] Ambacher O 1998 Growth and applications of Group III-nitrides *J. Phys. D: Applied Physics* **31** 2653-2710

[4] Liu L and Edgar J H 2002 Substrates for gallium nitride epitaxy *Mat. Sci. Engineer. R: Reports* **37** 61-127

[5] Krost A and Dadgar A 2002 GaN-based optoelectronics on silicon substrates *Mat. Sci. Engineer. B* **93** 77-84

[6] Eliashevich I, Li Y, Osinsky A, Tran C A, Brown M G and Karlicek K A, Jr. 1999 InGaN blue light-emitting diodes with optimized n-GaN layer *Proc. SPIE* **3621** 28-36

[7] Kim H, Lee J M, Huh C, Kim S W, Kim D J, Park S J, and Hwang H 2000 Modeling of a GaN-based light-emitting diode for uniform current spreading *Appl. Phys. Lett.* **77** 1903-4

[8] Guo X and Schubert E F 2001 Current crowding and optical saturation effects in GaInN/GaN light-emitting diodes grown on insulating substrates *Appl. Phys. Lett.* **78** 3337-9

[9] Guo X, Li Y L and Schubert E F 2001 Efficiency of GaN/InGaN light-emitting diodes with interdigitated mesa geometry *Appl. Phys. Lett.* **79** 1936-8

[10] Kim H, Park S and Hwang H 2002 Design and fabrication of highly efficient GaN-based light-emitting diodes *IEEE Trans. Electron Devices* **49** 1715-22

[11] Bulashevich K A, Evstratov I Yu, Mymrin V F and Karpov S Yu 2007 Current spreading and thermal effects in blue LED dice *Phys. Stat Solidi (c)* **4** 45-8

[12] Piprek J, Katona T, DenBaars S P and Li S 2004 3D simulation and analysis of AlGaN/GaN ultraviolet light-emittings diodes *Proc. SPIE* **5365** 127-36

[13] Evstratov I Yu, Mymrin V F, Karpov S Yu and Makarov Yu N 2006 Current crowding effects on blue LED operation *Phys. Stat. Solidi (c)* **3** 1645-8

[14] Monakhov A, Krier A and Sherstnev V V 2004 The effect of current crowding on the electroluminescence of InAs mid-infrared light emitting diodes *Semicond. Sci. Technol.* **19** 480-4

[15] Larson J W 2007 Some organising principles for coupling in multiphysics and multiscale models *Preprint ANL/MCS-P1414-0207*

[16] Chakraborty A, Shen L, Masui H, DenBaars S P and Mishra U 2006 Interdigitated multipixel arrays for the fabrication of high-power light-emitting diodes with very low series resistances *Appl. Phys. Lett.* **88** 181120

[17] Karpov S Yu 2007 Visible Light-Emitting Diode, In: *Nitride Semiconductor Devices: Principles and Simulation*, Ed. J. Piprek (Weinheim: WILEY-VCH Verlag GmbH and Co. KGaA) Ch.14, 303-325

[18] Eds. Leninshtein M E, Rumyantsev S L, and Shur M S, *properties of avdanced semiconductor materials: GaN, AlN, InN, BN, SiC, SiGe* (NY: John Willey and Sons, Inc.), chapter 1

[19] Slobodyan T E, Bulashevich K A, and Karpov S Y 2008 Optical Confinement in Laser Diodes Based on Nitrides of Group III Elements. Part 1: Theory and Optical Properties of Materials, *Semiconductors* **42** 845-51

[20] http://www.semitech.us/products/SimuLED/

[21] Shen Y C, Wierer J J, Krames M R, Ludowise M J, Misra M S, Ahmed F, Kim A Y, Mueller G O, Bhat J C, Stockman S A, and Martin P S 2003 Optical cavity effects in InGaN/GaN quantum-well-heterostructure flip-chip light-emitting diodes, *Appl. Phys. Lett.* **82** 2221-3

[22] Karpov S Yu and Makarov Yu N 2002 Dislocation effect on light emission efficiency in gallium nitride *Appl. Phys. Lett.* **81** 4721-3

[23] Bogdanov M V, Bulashevich K A, Evstratov I Yu, and Karpov S. Yu 2008 Current spreading, heat transfer, and light extraction in multi-pixel LED array, *Phys. Stat Solidi (c)* **6** 2070-2